0026-895X/05/6803-855–865$20.00
MOLECULAR PHARMACOLOGY
Copyright © 2005 The American Society for Pharmacology and Experimental Therapeutics
Mol Pharmacol 68:855–865, 2005

Vol. 68, No. 3
12278/3049770
Printed in U.S.A.

Intracellular K^+ Is Required for the Inactivation-Induced High-Affinity Binding of Cisapride to HERG Channels

Jijin Lin,[1] Jun Guo, Hongying Gang, Peter Wojciechowski, Jeffrey T. Wigle, and Shetuan Zhang

Institute of Cardiovascular Sciences, St. Boniface General Hospital Research Centre and Department of Physiology (J.L., J.G., H.G., P.W., S.Z.), and Division of Stroke and Vascular Disease, St. Boniface General Hospital Research Centre and Department of Biochemistry and Medical Genetics (J.L., J.T.W.), Faculty of Medicine, University of Manitoba, Winnipeg, Manitoba, Canada

Received February 24, 2005; accepted June 20, 2005

ABSTRACT

Many commonly used medications can cause long QT syndrome and thus increase the risk of life-threatening arrhythmias. High-affinity human *Ether-à-go-go*-related gene (HERG) potassium channel blockade by structurally diverse compounds is almost exclusively responsible for this side effect. Understanding drug-HERG channel interactions is an important step in avoiding drug-induced long QT syndromes. Previous studies have found that disrupting HERG inactivation reduces the degree of drug block and have suggested that the inactivated state is the preferential state for drug binding to HERG channels. However, recent studies have also shown that inactivation does not dictate drug sensitivity of HERG channels. In the present study, we examined the effect of inactivation gating on cisapride block of HERG. Modulation of HERG inactivation was achieved by either changing extracellular K^+ or Cs^+ concentrations or by mutations of the channel. We found that although inactivation facilitated cisapride block of the HERG K^+ current, it was not coupled with cisapride block of HERG when the Cs^+ current was recorded. Furthermore, cisapride block of the HERG K^+ current was not linked with inactivation in the mutant HERG channels F656V and F656M. Our results suggest that inactivation facilitates cisapride block of HERG channels through affecting the positioning of Phe-656.

The delayed rectifier potassium current (I_K) is the principal current responsible for cardiac repolarization. I_K is subdivided into the rapidly and slowly activating components I_{Kr} and I_{Ks}, respectively (Sanguinetti and Jurkiewicz, 1990). The human *Ether-à-go-go*-related gene (*HERG*), encodes the pore-forming subunit of the I_{Kr} channels (Sanguinetti et al., 1995; Trudeau et al., 1995). Reduction of I_{Kr} results in the prolongation of the cardiac action potential duration and causes the human long QT syndrome (LQTS) (Keating and Sanguinetti, 2001), a disorder of myocellular repolarization that predisposes affected persons to life-threatening ventricular tachyarrhythmia and sudden cardiac death (Keating and Sanguinetti, 2001). Congenital LQTS is relatively rare, but acquired LQTS is far more frequent and is a side effect of a variety of common medications. In theory, a reduction of any voltage-gated K^+ current that contributes to ventricular repolarization could cause LQTS. However, almost all known drugs that cause LQTS preferentially block the HERG channels (Roden et al., 1996; Mitcheson et al., 2000a). HERG blockade by different drugs represents one of the major concerns in drug safety. Thus, it is imperative to understand the molecular mechanisms that underlie drug-induced HERG channel block.

HERG displays a characteristic fast voltage-dependent inactivation gating. When depolarized, HERG channels open at a rate slower than that of inactivation (Smith et al., 1996; Spector et al., 1996). Upon repolarization, inactivated channels quickly reopen and then deactivate. Hence, depolarized HERG channels exist primarily in either the open or the inactivated state (Smith et al., 1996; Spector et al., 1996). Previous studies have shown that for most HERG-blocking agents, block develops only when the channel is depolarized (Kiehn et al., 1996; Snyders and Chaudhary, 1996; Zhang et al., 1999), suggesting that one or both of the depolarization-induced states (open versus inactivated) represent high-af-

This work was supported by Canadian Institutes of Health Research grant 7774, a grant from the Heart and Stroke Foundation of Manitoba, and an Establishment grant from Manitoba Health Research Council (to S.Z.). S.Z. is a recipient of the New Investigator Award from the Heart and Stroke Foundation of Canada. J.T.W. is a recipient of the New Investigator Award from the Canadian Institutes of Health Research.

[1] Current address: The first affiliated hospital, Shantou University Medical College, Shantou, China.

Article, publication date, and citation information can be found at http://molpharm.aspetjournals.org.
doi:10.1124/mol.105.012278.

ABBREVIATIONS: HERG, human *Ether-à-go-go*-related gene; LQTS, long QT syndrome; HEK, human embryonic kidney; PCR, polymerase chain reaction; I-V, current-voltage; WT, wild type.

finity states for drug binding. It has been found that mutations of HERG that disrupt inactivation reduce HERG block by E-4031, dofetilide, and verapamil (Ficker et al., 1998; Zhang et al., 1999), suggesting that the inactivated state forms the high affinity receptor for drug binding. However, a recent study suggested that the positioning of S6 aromatic residues relative to the central cavity of the channel, not inactivation per se, determines the drug block of HERG channels (Chen et al., 2002).

It has been reported that the elevation of extracellular K^+ concentration ($[K^+]_o$) relieves drug block of I_{Kr}/HERG channels (Yang and Roden, 1996; Wang et al., 1997). Because most HERG blockers access HERG channels from the cytosolic side of the membrane (Zhang et al., 1999, 2001; Mitcheson et al., 2000b), whether intracellular K^+ concentration ($[K^+]_i$) regulates drug binding to HERG channels is relevant.

In the present study, we used the well studied HERG blocker cisapride (Mohammad et al., 1997; Mitcheson et al., 2000a; Chen et al., 2002; Fernandez et al., 2004) to investigate the molecular mechanisms of drug-HERG channel interactions. Whole-cell patch-clamp technique (Zhang et al., 2003b) was used to record currents from the wild-type (WT) and mutant HERG channels heterologously expressed in HEK 293 cells. By using Cs^+ permeation and site-directed mutations, we have found that when intracellular K^+ was replaced by Cs^+ or when Phe-656 was mutated to valine or methionine, the cisapride block of HERG channels was no longer dependent on inactivation gating. We propose that inactivation re-orientates Phe-656 to a position that favors high-affinity binding of cisapride to HERG channels, and the presence of intracellular K^+ is required for this process.

Materials and Methods

Molecular Biology. We made three mutations in the pore and S6 region to assess the role of inactivation in the cisapride block of HERG channels. The S620T mutation was made to remove HERG inactivation gating (Ficker et al., 1998; Zhang et al., 1999). The F656V and F656M mutations were made to modify cisapride binding to HERG. The F656V and F656M mutations were selected for two reasons. First, the Phe-656 residue of HERG has been shown to be a molecular determinant of high-affinity dofetilide and cisapride binding (Lees-Miller et al., 2000; Mitcheson et al., 2000a). Second, these mutant channels have been shown to display properties that are similar to those of WT channels (Lees-Miller et al., 2000; Fernandez et al., 2004).

HERG cDNA in pCDNA3 was obtained from Dr. Gail A. Robertson (University of Wisconsin, Madison, WI) (Trudeau et al., 1995). Point mutations in the P-loop and S6 of HERG were introduced via PCR using overlap extension (Ho et al., 1989) (Table 1).

The forward and reverse flanking primers were designed to cover two unique restriction sites (BstEII at nucleotide 2038 and SbfI at nucleotide 3093). The first round of PCRs was performed using the forward flanking primer-reverse mutant primer and the reverse flanking primer-forward mutant primer. In the first round of PCRs, the total reaction volume was 50 μl, including 50 pmol of each primer, 70 ng of HERG cDNA, and 0.125 units of Vent DNA polymerase (New England Biolabs, Beverly, MA). Reaction temperatures were varied using a thermal cycler (MyCycler; Bio-Rad, Hercules, CA): 95°C for 120 s; 94°C for 60 s, 55°C for 60 s and 72°C for 60 s for 30 cycles; and 72°C for 10 min. The resulting PCR products were used as templates and amplified by flanking primers in a second round of PCR. The final PCR product was digested with BstEII and SbfI and ligated to HERG expression plasmid digested with the same two restriction enzyme sites. All mutations were verified by using a high-throughput 48 capillary ABI 3730 sequencer (UCDNA Services, University of Calgary, Calgary, AB, Canada).

HERG S620T, F656V, and F656M mutant channels were transiently expressed in HEK 293 cells (American Type Culture Collection, Manassas, VA). HEK 293 cells were seeded at 5×10^3 cells/60-mm diameter dish. The cells were transiently transfected using 10 μl of Lipofectamine with 4 μg of HERG mutant expression vector. After 24 to 48 h, at least 50% of cells expressed channels. Nontransfected HEK 293 cells contain a small-amplitude background current that is usually less than 100 pA upon a depolarizing pulse to 50 mV. Thus, the effects of overlapping endogenous currents of HEK 293 cells on the expressed current are minimal (Zhou et al., 1998).

A HEK 293 cell line stably expressing HERG channels was obtained from Dr. Craig January's lab (University of Wisconsin, Madison, WI) (Zhou et al., 1998), where the HERG cDNA (Trudeau et al., 1995, 1996) was subcloned into BamHI/EcoRI sites of the pCDNA3 vector (Invitrogen, Carlsbad, CA). The stably transfected cells were cultured in minimum essential medium supplemented with 10% fetal bovine serum and contained 400 μg/ml G418 to select for transfected cells. For electrophysiological study, the cells were harvested from the culture dish by trypsinization and stored in standard minimal essential medium at room temperature for later use. Cells were studied within 8 h of harvest.

Patch-Clamp Recording Method. The whole-cell, patch-clamp method was used. The pipette solution contained 135 mM KCl or CsCl, 5 mM EGTA, 1 mM $MgCl_2$, and 10 mM HEPES, pH adjusted to 7.2 with KOH or CsOH. The bath solution contained 10 mM HEPES, 10 mM glucose, 1 mM $MgCl_2$, 2 mM $CaCl_2$, and 135 mM NaCl and was adjusted to pH 7.4 with NaOH. For recordings in the presence of different external K^+ or Cs^+ concentrations, the concentration of Na^+ was reduced as the K^+ or Cs^+ concentration was elevated to maintain a constant osmolarity, and the pH was adjusted to 7.4 with the appropriate hydroxide solution. All chemicals were from Sigma (St. Louis, MO).

Aliquots of cells were allowed to settle on the bottom of a <0.5-ml cell bath mounted on an inverted microscope (TE2000; Nikon, Tokyo, Japan). Cells were superfused with specific bath solutions. The bath solution was constantly flowing through the chamber and the solution was changed by switching the perfusates at the inlet of the chamber. This bath solution change took 10 s. Patch electrodes were fabricated using thin-walled borosilicate glass (World Precision Instruments, Sarasota, FL). The pipette had an inner diameter of ~1.5 μm and a resistance of ~2 MΩ when filled with the pipette solution. An Axopatch 200B amplifier was used to record membrane currents. Computer software (pCLAMP9; Axon Instruments, Foster City, CA) was used to generate voltage clamp protocols, acquire data, and analyze current signals. Data were filtered at 5 to 10 kHz and sampled at 20 to 50 kHz for all protocols. In most cases, 80% series resistance compensation was used and leak subtraction was not used. Conductance/voltage data were fitted to a single Boltzmann

TABLE 1
Primers used for PCR reactions
Mutant nucleotides are underlined.

Primers	Sequence
Flanking	
Forward	CCACAATGTCACTGAGAAGGTCACCCAGG
Reverse	GCAGTGAGCGGTTCAGGTGCAGGCAGATGTC
S620T	
Forward	CTACTTCACCTTCAC<u>C</u>AGCCTCACCAGTGTGGG
Reverse	CCCACACTGGTGAGGCTG<u>G</u>TGAAGGTGAAGTAG
F656V	
Forward	ATGTATGCTAGCATC<u>G</u>TCGGCAACGTGTCGGC
Reverse	GCCGACACGTTGCCGAC<u>G</u>ATGCTAGCATACAT
F656M	
Forward	ATGTATGCTAGCATC<u>AT</u>GGGCAACGTGTCGGC
Reverse	GCCGACACGTTGCCC<u>AT</u>GATGCTAGCATACAT

function, $y = 1 / (1 + \mathrm{Exp}((V_{1/2} - V)/k))$, where y is the current normalized with respect to the maximal tail current, $V_{1/2}$ is the half-activation potential or mid-point of the activation curve, V is the voltage during the prepulse, and k is the slope factor, in millivolts, reflecting the steepness of the voltage dependence of gating. Concentration effects were quantified by fitting the data to the Hill equation ($I_{drug}/I_{control} = 1/[1 + (D/IC_{50})^{nH}]$, where D is the drug concentration, IC_{50} is the drug concentration for 50% block, and n_H is the Hill coefficient to the results. Data are given as mean ± S.E.M. Clampfit (Axon Instruments) and Origin (OriginLab Corp., Northampton, MA) were used for data analysis. Curve fitting was done using multiple nonlinear least-squares regression analysis. All experiments were performed at room temperature (23 ± 1°C).

Results

External K^+ and Inactivation Gating Regulate Cisapride Block of HERG Channels. Consistent with previous studies (Mohammad et al., 1997; Mitcheson et al., 2000a; Chen et al., 2002), we found that cisapride potently blocks HERG channels in a stably transfected HEK 293 cell line. Figure 1, A and B, shows families of current traces from one cell for control conditions (Fig. 1A) and after exposure to 100 nM cisapride (Fig. 1B). Figure 1C shows the current-voltage (I-V) relationships of the pulse currents measured at the end of depolarizing steps and the peak tail current before and after exposure to 100 nM cisapride, which markedly reduced the pulse and tail currents.

Changes in extracellular K^+ concentration ($[K^+]_o$) have been shown to influence the binding of drugs such as dofetilide and E-4031 to I_{Kr}/HERG channels (Yang and Roden, 1996; Wang et al., 1997). We found that the potency of cisapride block of the WT HERG channel was also strongly modulated by $[K^+]_o$ as demonstrated in Fig. 1, D and E. Figure 1D shows the superimposed currents before and after exposure to 50 nM cisapride in bath solutions containing 0, 5, or 135 mM K^+ with a pipette solution containing 135 mM K^+. From a holding potential of −80 mV, HERG currents were evoked by a depolarization to 50 mV for 4 s, followed by a step to −50 mV to record tail current. Because cisapride is reported to bind to HERG only after the channel opens (Mohammad et al., 1997), a series of depolarizing pulses was delivered every 15 s until a steady-state block was reached. The blocking effects were measured by the degree of peak tail current suppressions. The cisapride block of HERG is strongly $[K^+]_o$-dependent. As can be seen in Fig. 1D, 50 nM cisapride blocked ~80% of the current in the absence of $[K^+]_o$, ~60% at 5 mM $[K^+]_o$, and ~20% at 135 mM $[K^+]_o$. To obtain a concentration-dependent relationship for block of HERG current by cisapride, six to eight cells were studied at each drug concentration. Under each $[K^+]_o$ condition, the tail current peak amplitude was normalized to the respective control value and was plotted as relative current amplitude against cisapride concentration (Fig. 1E). Data points were fitted to

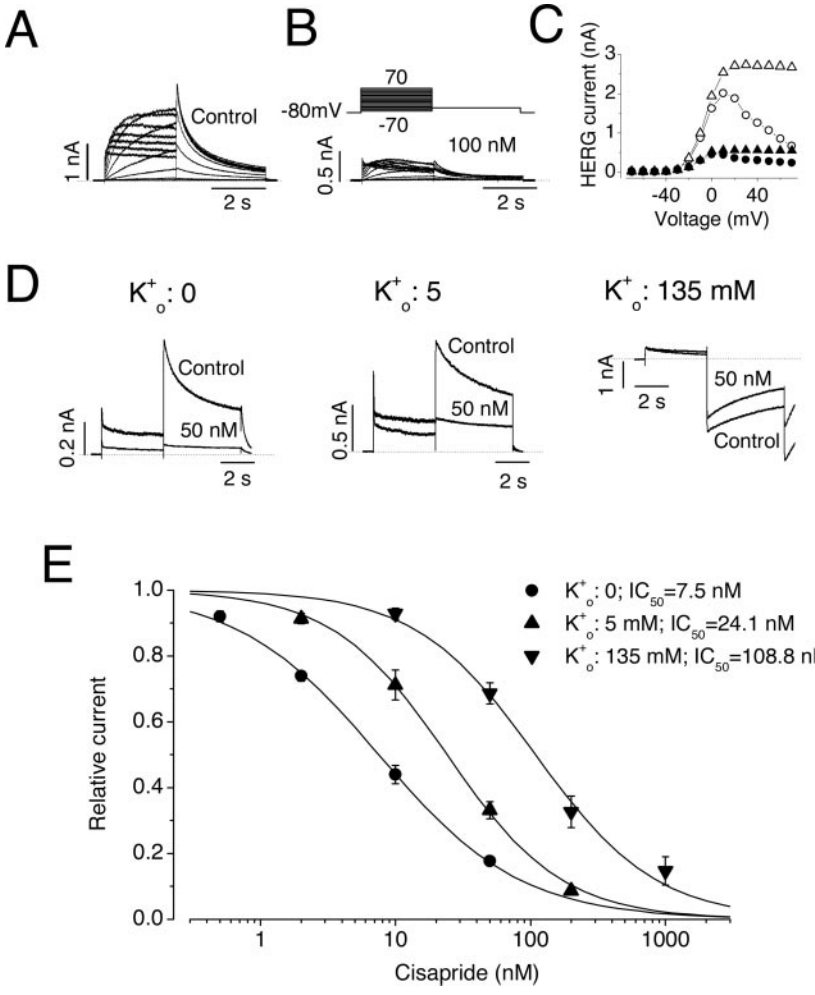

Fig. 1. Extracellular K^+ concentration (K^+_o) regulates the cisapride block of HERG K^+ currents. A and B, HERG currents recorded in the control condition (A) and after exposure to 100 nM cisapride (B). The pipette solution contained 135 mM K^+ and the bath solution contained 5 mM K^+. Voltage protocol is shown in the inset of B. The interpulse interval was 15 s. C, current-voltage plots of the pulse currents (○, ●) at the end of the 4-s depolarizing steps and the peak tail currents (△, ▲) before (○, △) and after (●, ▲) exposure to 100 nM cisapride. D, HERG K^+ currents recorded in the absence and presence of 50 nM cisapride at $[K^+]_o$ of 0, 5, or 135 mM. The currents were elicited by repetitive depolarizing steps to + 50 mV for 4 s followed by a repolarization to −50 mV to record the tail current. The holding potential was −80 mV. E, concentration-dependent block of HERG channels by cisapride at $[K^+]_o$ of 0 (●), 5 (▼), or 135 mM (▼).

the Hill equation. The half-maximal inhibition concentration (IC_{50}) for cisapride block of HERG current was 7.5 ± 0.8 nM at 0 $[K^+]_o$, 24.1 ± 1.2 nM at 5 mM $[K^+]_o$, and 108.8 ± 12.9 nM at 135 mM $[K^+]_o$. The IC_{50} values are significantly different from one another (n = 6–8 cells for each data point, $p < 0.01$). The corresponding Hill coefficients were 0.8, 1.0, and 1.0, respectively, suggesting that the occupation of a single binding site accounts for the block by cisapride.

Because $[K^+]_o$ regulates HERG inactivation and because inactivation has been shown to play an important role in high-affinity drug binding to HERG channels (Zhang et al., 1999, 2003a), we assessed the role of HERG inactivation in altering cisapride block at different $[K^+]_o$. We constructed an inactivation-deficient mutant HERG channel, S620T (Fig. 2). The S620T mutation lies in the S5-S6 linker of the channel pore. Previous studies have shown that this mutation interferes with the C-type inactivation and modifies the blocking of HERG channels caused by dofetilide, clofilium, and verapamil (Suessbrich et al., 1997; Ficker et al., 1998; Zhang et al., 1999). Consistent with these previous reports, we found that the conservative substitution of serine with threonine at position 620 resulted in a complete removal of inactivation. Figure 2, A and B, shows families of the S620T currents from one cell for control conditions (Fig. 2A) and after exposure to cisapride (Fig. 2B). The cell was clamped at a holding potential of −80 mV. Depolarizing steps were applied for 4 s to voltages between −70 and +70 mV in 10-mV increments. For control conditions, depolarizing steps activated a time-dependent outward current that increased in amplitude as voltage steps became more positive. The inward rectification seen in WT HERG channels was absent (Fig. 2C). In the presence of 100 nM cisapride, the S620T current displayed a time-dependent decay during the depolarizing steps (Fig. 2B). Cisapride has been shown to preferentially block activated (open) channels (Mohammad et al., 1997). Therefore, the decay reflects time-dependent drug binding to open channels. Because release of cisapride block occurs during the resting potential, the time-dependent block could be observed upon each depolarization (Mohammad et al., 1997; Zhang et al., 1999). Figure 2C shows the I-V relationship of currents measured at the end of depolarizing steps in control and in the presence of 100 nM cisapride.

The cisapride block of HERG S620T channels and its $[K^+]_o$ dependence were studied in Fig. 2, D and E. HERG channels were activated by a depolarizing pulse to +50 mV for 4 s every 15 s. There was no clear sign of inactivation in control recordings. Unlike WT channels, the S620T mutant channel was blocked by cisapride in a $[K^+]_o$-independent manner. The steady-state block measured at the end of a 4-s depolarizing step under each cisapride concentration was normalized to its control value. Four to seven cells were studied at each concentration, and the blocking effects were plotted against cisapride concentrations. The data were fitted to the Hill equation. The IC_{50} for cisapride at $[K^+]_o$ of 0, 5, or 135

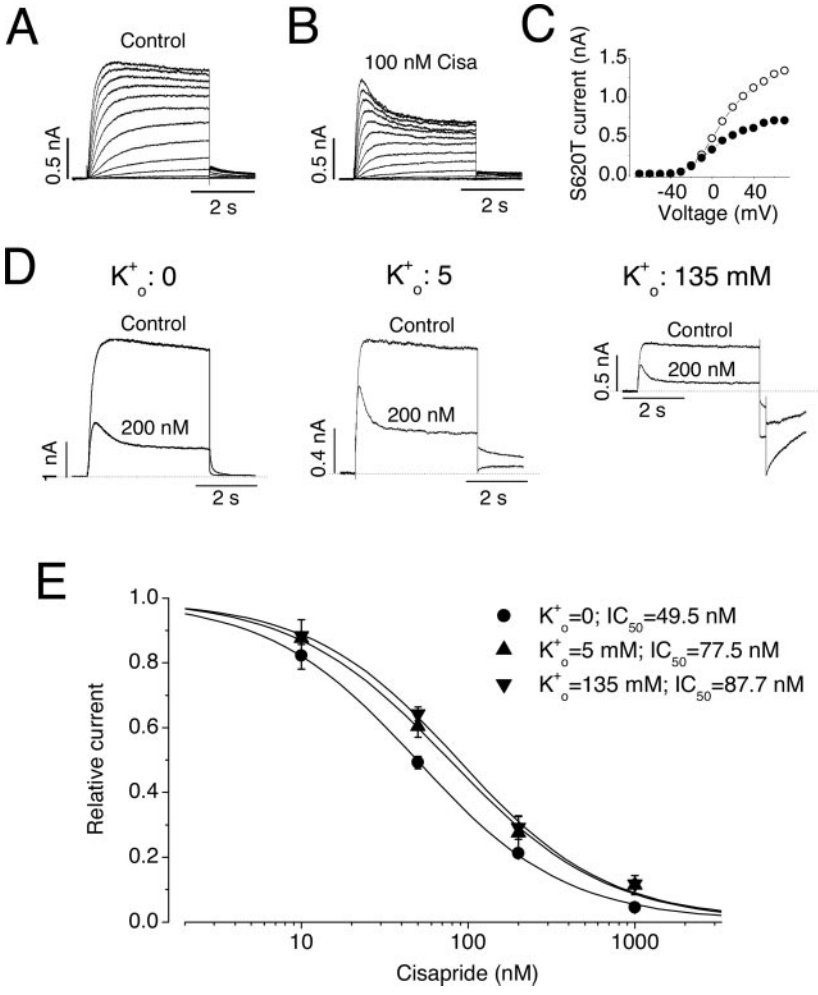

Fig. 2. The S620T mutation reduces cisapride block and eliminates the $[K^+]_o$ dependence of the cisapride block of HERG channels. A and B, the HERG S620T currents recorded in the control condition (A) and after exposure to 100 nM cisapride (B). The pipette solution contained 135 mM K^+ and bath solution contained 5 mM K^+. Voltage protocol was the same as shown in the inset of Fig. 1B. C, the current-voltage relationship of the pulse currents at the end of 4-s depolarizing steps before (○) and after (●) exposure to 100 nM cisapride. D, the HERG S620T currents for control and in the presence of 200 nM cisapride at $[K^+]_o$ of 0, 5, or 135 mM. Currents were elicited by a depolarization to +50 mV for 4 s followed by a repolarization to −50 mV. At $[K^+]_o$ of 135 mM, the repolarization to −50 mV was brief (200 ms). The holding potential was −80 mV. E, concentration dependence of cisapride block of S620T channels. The current amplitude at the end of 4-s depolarization to 50 mV was normalized to the control, plotted against cisapride concentrations, and fitted to the Hill equation.

mM was 49.5 ± 2.1, 77.5 ± 6.0, and 87.7 ± 11.5 nM, respectively (n = 4–7 cells). The Hill coefficients for the fits were 1.0, 1.2, and 1.0 at 0, 5, or 135 mM $[K^+]_o$, respectively.

Two observations are obvious. First, the S620T mutation reduced the sensitivity of the HERG channel to cisapride. For example, at $[K^+]_o$ of 0, the IC_{50} of cisapride block of S620T was 49.5 nM, which is significantly higher than the IC_{50} (7.5 nM) for the WT channels ($P < 0.01$). Second, compared with WT channels, the $[K^+]_o$ dependence of cisapride block was significantly diminished in the S620T mutant channel. For example, whereas changing $[K^+]_o$ from 135 mM to 0 increased cisapride block in the WT channel by 14.5-fold, the same decrease in $[K^+]_o$ increased cisapride block of the S620T channel by only 1.8-fold ($p < 0.01$). These results indicate that the $[K^+]_o$ dependence of cisapride block of the WT HERG channel is largely related to the ability of $[K^+]_o$ to slow HERG inactivation gating.

Cisapride Block of HERG Cs^+ Current Is Independent of Inactivation Gating. We have found that HERG channels display a unique high permeability to Cs^+ (Zhang et al., 2003a). Because cisapride blocks HERG by binding to the internal cavity of the channel (Mitcheson et al., 2000a), we hypothesized that intracellular K^+ ($[K^+]_i$) may play a role in drug binding to the HERG channel. We reasoned that intracellular Cs^+ (Cs^+_i) may differ from $[K^+]_i$ in regulating the drug-HERG interactions, and we investigated the effects of cisapride on the HERG Cs^+ current. A pipette solution containing 135 mM Cs^+ and a bath solution containing various Cs^+ concentrations (Na^+ as substitute) were used to study the effects of extracellular Cs^+ on cisapride block. The WT HERG Cs^+ currents display features very similar to those of K^+ currents, except there is a larger outward current peak upon depolarization which decays quickly as channels inactivate (see Fig. 5A for the current voltage relationships of Cs^+ current). Cisapride blocked HERG Cs^+ current in a concentration dependent manner. However, as shown in Fig. 3, in contrast to that of the K^+ current, cisapride block of HERG Cs^+ current was entirely independent of extracellular Cs^+ concentration ($[Cs^+]_o$) which has been shown to slow HERG inactivation gating (Zhang et al., 2003a). The IC_{50} for cisapride at $[Cs^+]_o$ of 0, 5, or 135 mM was 173.6 ± 12.6, 191.5 ± 9.4, and 195.6 ± 20.6 nM, respectively (n = 4–7 cells). The corresponding Hill coefficients were 1.3, 0.9, and 1.0, suggesting that the occupation of a single binding site accounts for the block of HERG Cs^+ current by cisapride.

To address the effect of $[Cs^+]_o$ on the inactivation time course of the Cs^+ current, HERG Cs^+ current was fully activated and inactivated by a depolarizing step to +40 mV for 500 ms. The cell was then repolarized to −100 mV for 10 ms to allow recovery from inactivation but not enough to allow significant deactivation of the HERG channels (Smith et al., 1996; Spector et al., 1996; Zhang et al., 2003a). A test step was then applied to different voltages to observe inactivation time courses every 15 s. The inactivation time constant (τ_{inact}) was obtained by fitting the current decay to a single exponential function. Data in Fig. 4, A–C, show HERG Cs^+ currents during the test steps to voltages between +20 and 120 mV in 20 mV increments at 0 (A), 5 (B), or 135 mM $[Cs^+]_o$ (C). The expanded traces during the test pulses are shown in Fig. 4, D–F. The averaged τ_{inact} in 0 (○), 5 (●), and

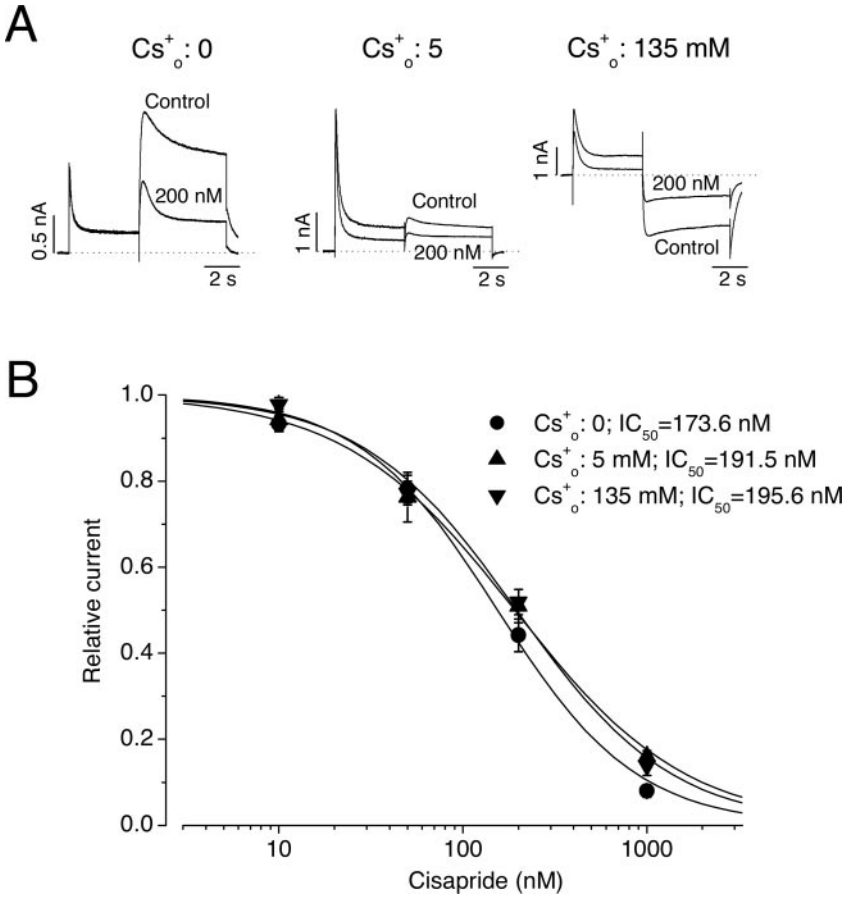

Fig. 3. Extracellular Cs^+ concentration ($[Cs^+]_o$) does not regulate cisapride block of HERG Cs^+ currents. Whole-cell Cs^+ currents were recorded with a pipette solution containing 135 mM Cs^+ and bath solutions containing 0, 5, or 135 mM Cs^+. A, Cs^+ current recorded in absence and presence of 200 nM cisapride at $[Cs^+]_o$ of 0, 5, and 135 mM. The currents were elicited by depolarizations to +50 mV from a holding potential of −80 mV. The depolarization was followed by a repolarization to −50 mV to record the tail currents. B, concentration-dependent block of HERG Cs^+ currents by cisapride. The tail current peak amplitudes at −50 mV were normalized to the control and plotted versus cisapride concentration. Fits to data points at 0 (●), 5 (▲), or 135 mM $[Cs^+]_o$ (▼) to the Hill equation are shown.

135 mM $[Cs^+]_o$ (▲) in five to eight cells are plotted as a function of test potential in Fig. 4G. Elevated $[Cs^+]_o$ slowed HERG Cs^+ current inactivation at all voltages tested. For example, τ_{inact} at 60 mV increased from 6.7 ± 0.9 ms in the absence of $[Cs^+]_o$ ($n = 8$) to 23.2 ± 5.7 ms at 5 mM $[Cs^+]_o$ ($n = 7$, $p < 0.01$), and to 198.7 ± 23.6 ms at 135 mM $[Cs^+]_o$ ($n = 5$, $p < 0.01$). Thus, elevation of $[Cs^+]_o$ markedly slowed HERG inactivation. The effects of $[Cs^+]_o$ on the voltage dependence of steady-state inactivation were also studied. To construct the steady-state inactivation, ratios of the current measured 100 ms after the onset of inactivation relative to instantaneous peak current at each test potential were calculated. The ratios were normalized to the maximal value, plotted as a function of the test voltage, and fitted to a Boltzmann function (Fig. 4H). Data were obtained from five to eight cells. The half-inactivation voltage and slope factor were −7.9 ± 0.7 and 16.2 ± 0.7 mV at 0 $[Cs^+]_o$, 5.6 ± 0.6 and 16.7 ± 0.6 mV at 5 mM $[Cs^+]_o$, and 24.7 ± 1.2 and 15.1 ± 1.3 mV at 135 mM $[Cs^+]_o$, respectively. Elevation of $[Cs^+]_o$ significantly shifted the midpoint of the steady-state inactivation curve to more depolarized potentials ($p < 0.01$) without significantly affecting the slope factor ($p > 0.05$). These results demonstrated that changing $[Cs^+]_o$ significantly slowed HERG inactivation but did not affect cisapride block of the Cs^+ current. Therefore, cisapride block and inactivation gating was not coupled in HERG Cs^+ current recordings.

To further evaluate the role of inactivation in the cisapride block of the HERG Cs^+ current, effects of cisapride on the WT and S620T Cs^+ currents were compared (Fig. 5). The pipette solution contained 135 mM Cs^+ and the bath solution contained 0 Cs^+ (Na^+ ions as substitute). To record current-voltage relationships, HERG Cs^+ current was elicited by depolarizing steps to voltages between −70 and 70 mV for 4 s followed by a repolarizing step to −50 mV (Fig. 5, A and B, top). The holding potential was −80 mV. Figure 5A shows the data from WT channels. The upper left shows a family of WT HERG Cs^+ currents in control, and the upper right shows the currents in the presence of 1 μM cisapride. HERG Cs^+ currents were measured at the end of depolarizing steps to construct the I-V relationship (Fig. 5A, bottom, $n = 6$ cells). In control conditions, the HERG current was activated at voltages positive to −50 mV, and a maximum current was reached at −10 mV. With more positive voltages, the inward rectification was apparent because of the voltage-dependent rapid inactivation. Cisapride (1 μM) nearly completely blocked the HERG Cs^+ current. Figure 5B shows the recordings from the inactivation-deficient mutant channel S620T. The top left shows a family of S620T HERG Cs^+ currents in control. The top right shows the currents in the presence of 1 μM cisapride. The S620T Cs^+ current was measured at the end of 4-s depolarizing steps to construct the I-V relationship (Fig. 5B, bottom, $n = 4$ cells). The inactivation of Cs^+ current has been largely removed by the S620T mutation. The S620T Cs^+ current was activated at voltages positive to −40 mV. In contrast to the WT channel, the amplitudes of the S620T currents at the end of 4-s depolarizing pulse became larger as the depolarization was more positive. The inward rectification was absent. However, similar to the WT channel, 1 μM

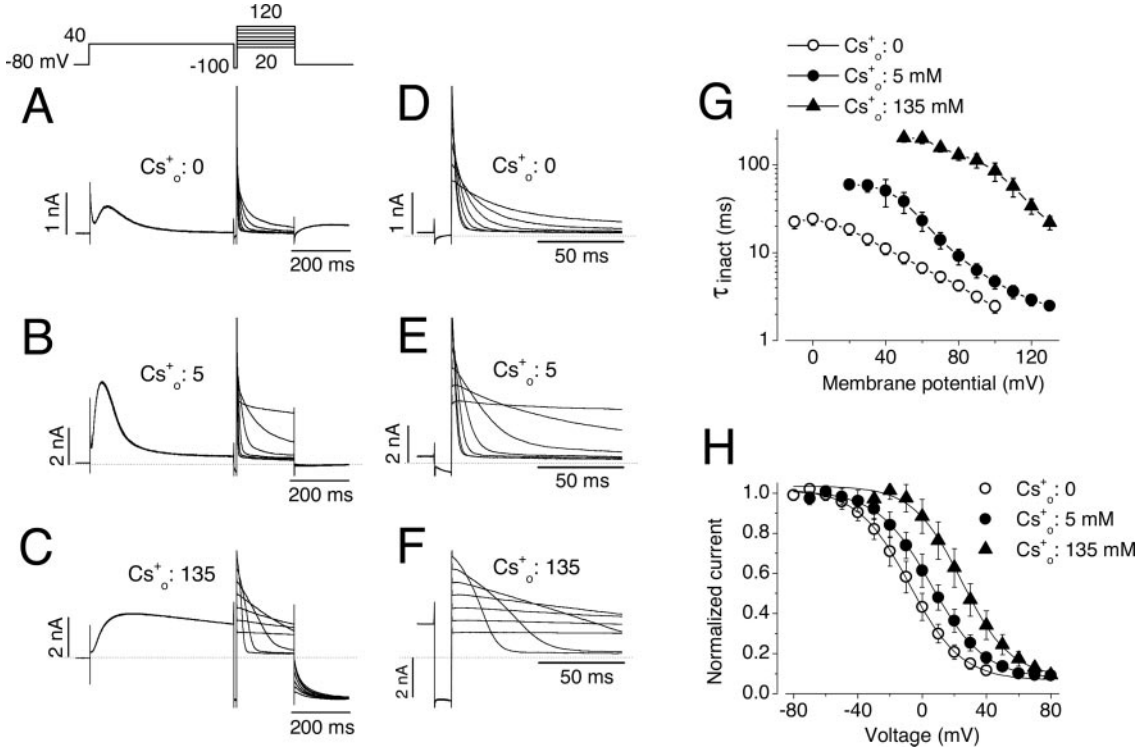

Fig. 4. Effects of $[Cs^+]_o$ on HERG Cs^+ current inactivation. HERG Cs^+ currents were elicited by the voltage protocol shown at the top of the figure. The pipette solution contained 135 mM Cs^+ and the external solutions contained 0 (A), 5 (B), or 135 mM Cs^+ (C). A 500-ms pulse to 40 mV to activate and inactivate HERG was followed by a 10-ms pulse to −100 ms to recover inactivated channels to open state. Test steps were then applied to voltages varying between 20 and 120 mV in 20-mV increments to record the time course of inactivation, which have been expanded in D, E, and F, respectively. The current decay at test voltages was fitted to a single exponential function to obtain the inactivation time constant (τ_{inact}). G, voltage dependence of τ_{inact} in external solutions containing 0 (○), 5 (●), or 135 mM (▲) $[Cs^+]_o$. Each point is the mean ± S.E.M. for five to eight cells. H, the steady-state inactivation of the Cs^+ current at 0 (○), 5 (●), or 135 mM (▲) $[Cs^+]_o$. Elevation $[Cs^+]_o$ significantly slowed the inactivation time course and shifted the steady-state inactivation to the depolarized direction ($n = 5–8$ cells, $P < 0.01$).

cisapride almost completely blocked the S620T Cs^+ current. To quantify the potency of cisapride block of HERG current, the concentration-dependent relationships were constructed with four to six cells studied at each drug concentration. For WT channels, HERG channels were activated and inactivated by a depolarization to 50 mV, the peak tail current upon repolarization to −50 mV was recorded to measure the channel block. For S620T channels, block was measured by current amplitudes at the end of a depolarizing step to 50 mV. The current amplitudes in the presence of cisapride were normalized to the control and plotted against cisapride concentration (Fig. 5C). Data points were fitted to the Hill equation. The IC_{50} for the WT and S620T channels were 173.6 ± 12.6 nM (n = 6) and 194.9 ± 19.6 nM (n = 4) with a Hill coefficient of 1.3 and 0.9, respectively. These concentration-dependent relationships were similar. Thus, in contrast to the K^+ current, the blocking of the HERG Cs^+ current by cisapride is independent of the inactivation gating.

Phe-656 of HERG Is Involved in the Inactivation-Facilitated Cisapride Block of K^+ Current. Our results thus far have demonstrated that when $[K^+]_i$ is replaced by $[Cs^+]_i$, cisapride block of HERG is no longer affected by HERG inactivation gating. This indicates a critical role of $[K^+]_i$ in the state-dependence of cisapride binding to HERG channels. Phe-656 has been shown to be critical for cisapride binding to HERG channels (Mitcheson et al., 2000a). We hypothesized that the positioning of Phe-656 may differ between open and inactivated state, and this may affect the binding of cisapride to HERG channels. The positioning of Phe-656 may be influenced by the types of the permeating ions. Therefore, K^+ and Cs^+ will result in different Phe positioning, ultimately affecting cisapride binding. When Cs^+ is permeating the channel, the optimal positioning of Phe-656 for cisapride binding may be less favored. To test the role of Phe-656 in the inactivation-induced changes of drug affinity, we mutated phenylalanine at 656 to valine or methionine. Figure 6 shows the activation properties of the HERG F656V (A–C) and F656M (D–F). The currents were recorded in 135 mM $[K^+]_i$ and 5 mM $[K^+]_o$ by 4-s depolarizing steps to voltages between −70 and +70 mV. The holding potential was −80 mV. Figure 6B shows the I-V relationship of the F656V pulse currents. The outward currents measured at the end of 4-s depolarizing pulses were plotted against depolarizing voltages. The HERG F656V current was activated at voltages positive to −50 mV, and the maximum current was reached at 0 mV. At more positive voltages, inward rectification was apparent because of the rapid voltage-dependent inactivation (Smith et al., 1996; Spector et al., 1996; Zhang et al., 1999). Figure 6C shows the activation curve for the F656V channel. Tail current amplitude was used to construct the activation curve (n = 5 cells), which shows that the threshold voltage for the F656V channel activation was close to −40 mV. The channels were fully activated at voltages >20 mV. When fitted to a Boltzmann function, the half-maximum activation voltage ($V_{1/2}$) and slope factor (k) were −10.1 ± 2.7 mV and 8.7 ± 0.6, respectively. These values are not significantly different from those in WT channels ($V_{1/2}$, −11.1 ± 4.0 mV; k, 7.9 ± 0.7 mV). To assess deactivation of the F656V channel, the decay of tail currents at −50 mV were fitted to double exponential functions. The fast and slow components of deactivation time constants (τ_{deact}) at −50 mV were 186.1 ± 13.4 and 723.9 ± 42.3 ms (n = 5), respectively. The fast component accounted for 0.59 of the current amplitude. For WT channels, the fast and slow components of τ_{deact} at −50 mV were 370.5 ± 18.9 and 1762.2 ± 156.5 ms (n = 6), respectively. The fast component accounted for 0.47 of the current amplitude. Therefore, the F656V channel displayed a significantly faster deactivation than the WT channel (n = 5 or 6, $p < 0.01$).

Figure 6, E and F, shows the I-V relationship (E) and the activation curve of F656M (F). The $V_{1/2}$ and slope factor were −17.1 ± 3.7 mV and 7.2 ± 0.4, respectively (n = 5). Although the $V_{1/2}$ of F656M displayed a moderate but significant shift to the negative potentials ($p < 0.05$), the slope factor of F656M was not different from that of WT channels. The deactivation time course of F656M was evaluated at −50 mV. The fast and slow components of τ_{deact} at −50 mV were 385.4 ± 45.1 and 2092.4 ± 190.8 ms, respectively (n = 5). The fast component accounted for 0.42 of the current amplitude.

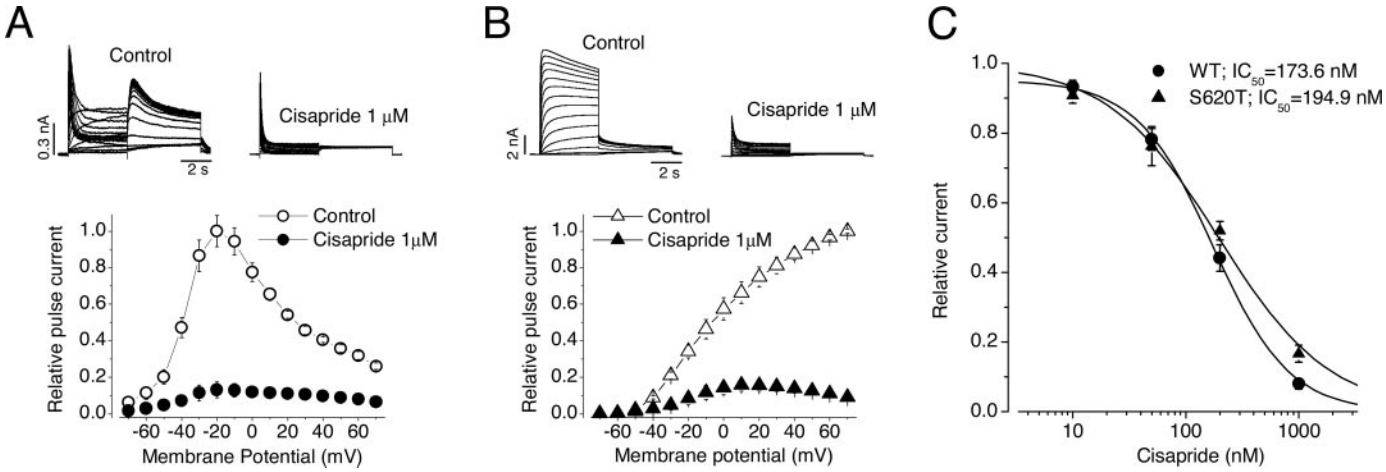

Fig. 5. Block of the HERG Cs^+ current by cisapride is not dependent on inactivation. The Cs^+ currents from WT and S620T channels were recorded with a pipette solution containing 135 mM Cs^+ and a bath solution containing 140 mM NaCl. A and B, The Cs^+ currents recorded in absence and presence of 1 μM cisapride in the WT (A) and S620T HERG channels (B). Top, families of currents. The current amplitudes at the end of each depolarizing pulse were normalized to the largest amplitude and plotted against each depolarization voltage to obtain normalized I-V relationships, which are shown at the bottom. C, concentration dependence of cisapride block of HERG Cs^+ currents in the WT (●) and S620T channels (▲). Cisapride blocked the WT and S620T Cs^+ currents with a similar potency.

These values were not significantly different from those of WT channels.

Figure 7 compares the inactivation properties of WT channels (A), F656V (B) and F656M mutant channels (C). Figure 7*a* shows the voltage dependence of the inactivation time course of K^+ currents from WT, F656V, and F656M at 5 mM $[K^+]_o$. The inactivation time constant (τ_{inact}) was obtained by fitting the currents to a single exponential function at each test voltage. The averaged τ_{inact} in 0, 5, and 135 mM $[K^+]_o$ (n = 6–8 cells) are plotted against test potentials in Fig. 7*b*. Although there was no significant difference in the τ_{inact} between the WT and F656V channels, τ_{inact} was significantly smaller for the F656M channel. For example, the mean time constants at 20 mV in the absence of $[K^+]_o$ were 9.2 ± 0.9, 7.4 ± 1.2, and 6.3 ± 0.4 ms for WT, F656V, and F656M channels, respectively (n = 5~6 cell each, $p > 0.05$ between WT and the F656V, and $p < 0.05$ between WT and the F656M). Despite the small difference of τ_{inact} between WT and the F656M channel, elevation of external K^+ caused a similar slowing of the inactivation time course in the WT, F656V, and F656M channels. Fig. 7*c* shows the steady-state inactivation relationships at different $[K^+]_o$ of WT, F656V, and F656M channels. The data were fitted to a Boltzmann function. The half-inactivation voltage ($V_{1/2}$) and slope factor (k) values are summarized in Table 2. Although the inactivation properties of F656V were similar to those of WT channels, the $V_{1/2}$ for the F656M was significantly more negative than that of WT (n = 5, $p < 0.01$). However, despite a moderately accelerated inactivation for the F656M channel, elevation of $[K^+]_o$ caused a similar shift of the steady-state inactivation in the WT, F656V, and F656M channels to the depolarized direction without significantly affecting the slope factors.

Consistent with the concept that Phe-656 is a critical site for drug binding, both F656V and F656M affected cisapride binding to the channel (Fig. 8). Although the F656V mutation significantly reduced cisapride affinity, the F656M had only a modest effect. We found that cisapride block of both F656V and F656M channels was not affected by changes of $[K^+]_o$ which modulate inactivation gating of both channels (see Fig. 7). The IC_{50} for cisapride block of F656V at 0, 5, or 135 mM $[K^+]_o$ was 99.9 ± 7.5, 101.1 ± 5.7, and 134.3 ± 13.2 nM, respectively ($p > 0.05$, n = 4–7 cells). The corresponding Hill coefficients were 1.2, 1.3, and 1.0, respectively. The IC_{50} for cisapride block of F656M at 0, 5, or 135 mM $[K^+]_o$ was 27.6 ± 2.1, 30.6 ± 4.1, and 34.0 ± 2.8 nM, respectively ($p > 0.05$, n = 4). The corresponding Hill coefficients were 1.3, 1.3, and 0.9.

Discussion

The exact role of inactivation in mediating drug block of HERG is not well understood. In the present study, we found that cisapride block of HERG was significantly attenuated by the impairment of inactivation gating. First, elevation of $[K^+]_o$, which slows inactivation, reduced the degree of cisapride block. Second, the inactivation deficient mutant S620T had a reduced cisapride affinity. Site-directed mutagenesis has identified aromatic residues, particularly Phe-656 in the S6 transmembrane domain of HERG subunits, to be one of the most important molecular determinants of high-affinity binding to HERG channels for many drugs such as MK-499, dofetilide, cisapride, terfenadine, quinidine, and chloroquine (Lees-Miller et al., 2000; Mitcheson et al., 2000a). To assess whether the facilitation of cisapride binding by inactivation gating is via the Phe-656 site, we evaluated the effects of $[K^+]_o$ on cisapride block of F656V and F656M channels. We reasoned that if Phe-656 is involved in the inactivation-induced facilitation of cisapride binding to HERG channels, changing inactivation gating by $[K^+]_o$ might differently affect the IC_{50} of HERG F656V and F656M. Indeed, we found that block of both mutant channels by cisapride was not affected by changing $[K^+]_o$, indicating that Phe-656 is involved in the inactivation-induced high-affinity binding of cisapride to HERG channels. The loss of $[K^+]_o$ regulation of cisapride-

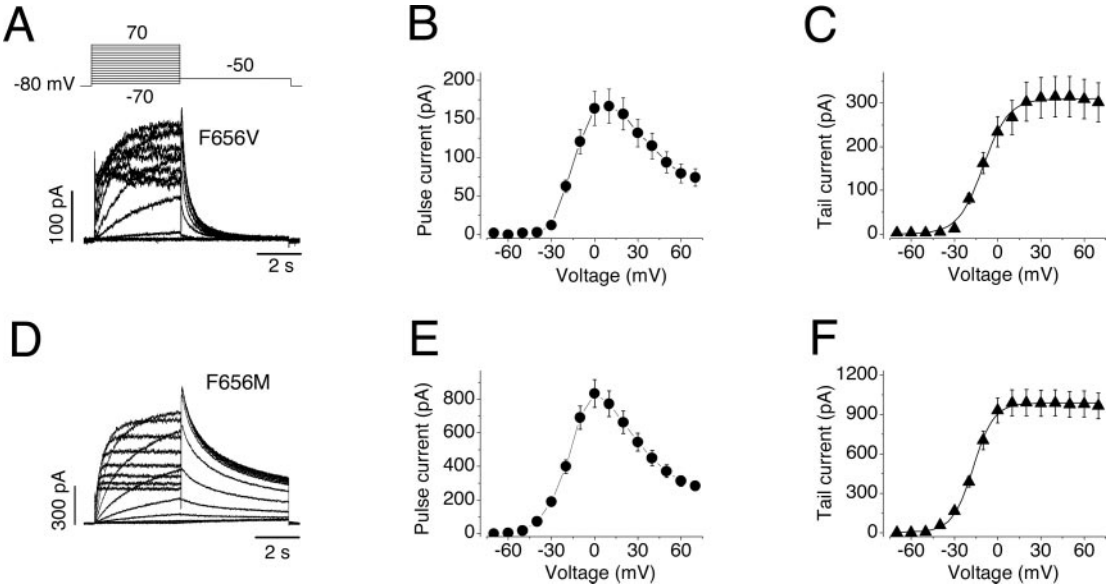

Fig. 6. Activation properties of the F656V and the F656M channel. A, a family of the F656V K^+ currents (135 mM $[K^+]_i$ and 5 mM $[K^+]_o$). B, I-V plot of the F656V currents measured at the end of depolarizing steps. C, activation curve of the F656V constructed based on the tail currents. The activation curve was fitted to a Boltzmann relationship. D, a family of the F656M K^+ currents. E, I-V plot of the F656M currents measured at the end of depolarizing steps. C, activation curve of the F656M channel.

mediated block of F656V and F656M channels does not result from the altered drug sensitivity of the mutant channels. In our study, the F656V HERG mutation displayed reduced cisapride sensitivity, but the F656M mutant channel displayed cisapride sensitivity similar to that of WT channels at 5 mM $[K^+]_o$. The difference of the cisapride affinity between the F656V and F656M seems to be related to the measures of hydrophobicity at the position 656. The potency for block of HERG by cisapride, terfenadine, and MK-499 correlate well with measures of hydrophobicity, especially the two-dimensional approximation of the van der Waals hydrophobic surface area of the side chain of residue 656 (Fernandez et al., 2004). The van der Waals hydrophobic surface area of methionine more closely resembles that of phenylalanine than does the hydrophobic surface area of valine (Fernandez et al., 2004). However, although the methionine residue mimics more closely the phenylalanine residue with regard to hydrophobicity, both methionine and valine lack the aromatic ring of phenylalanine, which may be important for the inactivation-facilitated cisapride binding to the channel. Based on the crystal structure of the KcsA K^+ channel (Doyle et al., 1998), Phe-656 of HERG (Thr-107 in KcsA) faces the central cavity of the intracellular mouth of the channel. The presence of a phenylalanine at this site in HERG seems to be important in creating a binding site for dofetilide, quinidine, MK-499, terfenadine, and cisapride (Lees-Miller et al., 2000; Mitcheson et al., 2000a). These compounds consist of an aliphatic chain with benzene rings at each end. Benzene rings are known to stack via π bonds, and it is possible that the benzene head groups of cisapride could interact with the

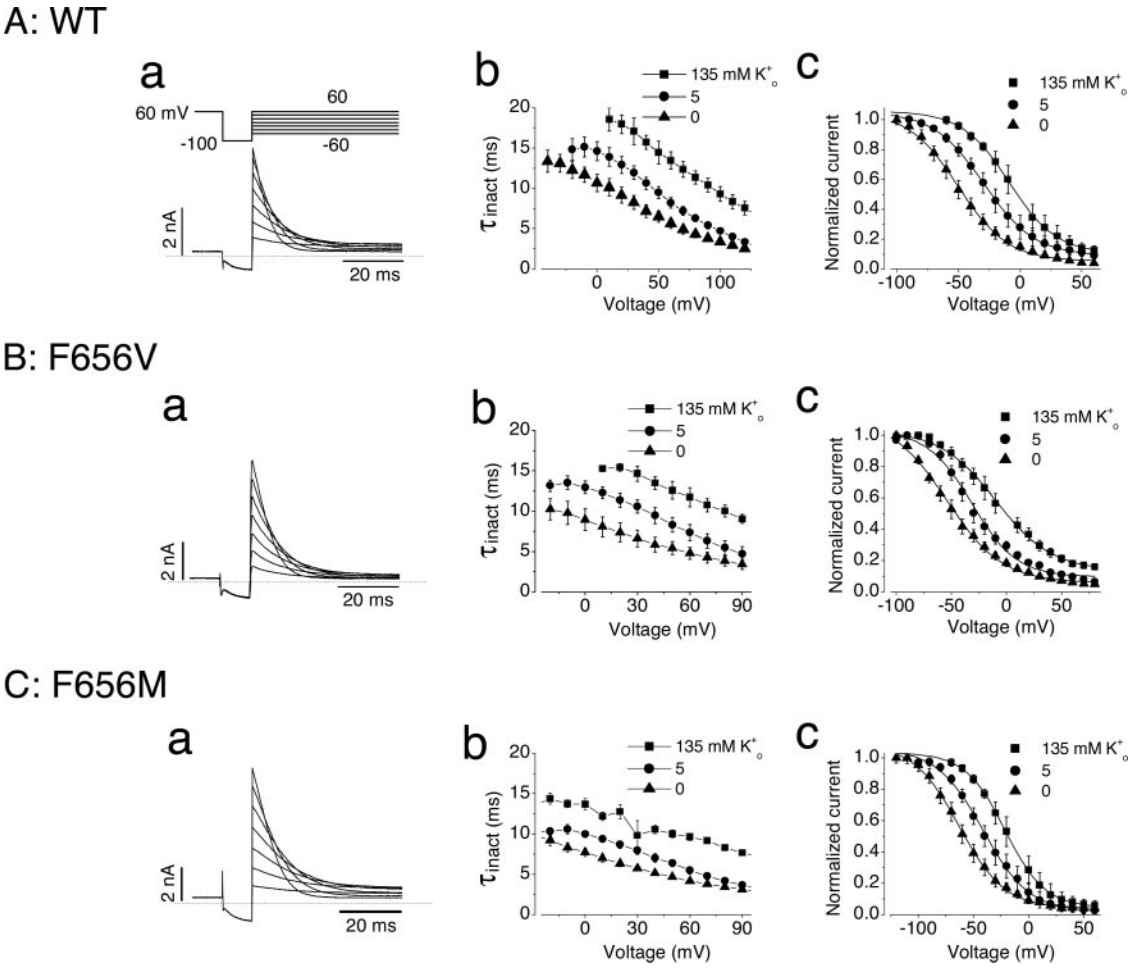

Fig. 7. Effects of $[K^+]_o$ on the inactivation time constants in the WT, F656V and F656M channel. In a, a voltage protocol, shown at the top, was used to record the time courses of inactivation. The inactivation time constant (τ_{inact}) was obtained by fitting the current decay to a monoexponential function. b, the τ_{inact}-voltage relationships at 0, 5, and 135 mM $[K^+]_o$. c, steady-state inactivation at 0, 5, and 135 mM $[K^+]_o$. The half-inactivation voltage and slope factor are summarized in Table 2.

TABLE 2
The steady-state inactivation parameters of the WT, F656V, and F656M channels at 0, 5 and 135 mM $[K^+]_o$

	0 mM $[K^+]_o$			5 mM $[K^+]_o$			135 mM $[K^+]_o$		
	$V_{1/2}$	k	n	$V_{1/2}$	k	n	$V_{1/2}$	k	n
WT	−50.1 ± 2.2	20.1 ± 1.1	6	−29.4 ± 1.4	20.6 ± 0.4	7	−8.9 ± 1.8	19.2 ± 1.2	5
F656V	−54.2 ± 4.1	25.2 ± 1.5	4	−33.1 ± 3.1	22.1 ± 1.9	5	−9.7 ± 2.9	25.1 ± 2.7	5
F656M	−62.9 ± 2.9*	21.6 ± 1.2	4	−41.4 ± 1.6*	20.9 ± 1.8	6	−19.1 ± 2.6*	19.1 ± 2.1	4

$V_{1/2}$, voltage for half-maximal inactivation; k, slope factor; n, number of cells tested.
* $P < 0.01$.

benzene ring of phenylalanine. Because of the structural nature, we propose that the positioning of the benzene ring of phenylalanine is more likely to be affected by the channel's inactivation gating, which affects drug binding. On the other hand, the positioning of the methionine residue may be less likely to be affected by the inactivation gating. Therefore, although F656M displayed cisapride sensitivity similar to that of the WT channels, it lost the $[K^+]_o$ dependence of the cisapride block.

The loss of $[K^+]_o$ regulation of cisapride-mediated block of F656V and F656M channels seems not to have been caused by the altered channel gating behaviors. The inactivation properties of F656V were similar to those of WT channels, whereas the F656M displayed a slightly accelerated inactivation. Like WT channels, elevation of $[K^+]_o$ significantly slowed inactivation of both F656V and F656M mutant channels. We have found that the F656M mutation moderately shifted the activation curve to hyperpolarized potentials. This result is consistent with data presented in a previous report (Fernandez et al., 2004). We also found that the activation properties of F656V were not altered, but deactivation of the F656V was significantly faster than WT channels. The finding of the accelerated deactivation of the F656V is consistent with the previous studies (Lees-Miller et al., 2000; Fernandez et al., 2004). It seems that the accelerated deactivation may not be the primary cause for the reduction in drug sensitivity for the F656V. The F656W mutation significantly alters the voltage dependence of activation/deactivation gating, but this mutation does not significantly alter the IC_{50} values for the block by MK-499, cisapride, and terfenadine (Fernandez et al., 2004).

The present study also revealed that the intracellular K^+ is involved in modulating cisapride binding during inactivation gating. We found that when Cs^+ replaces intracellular

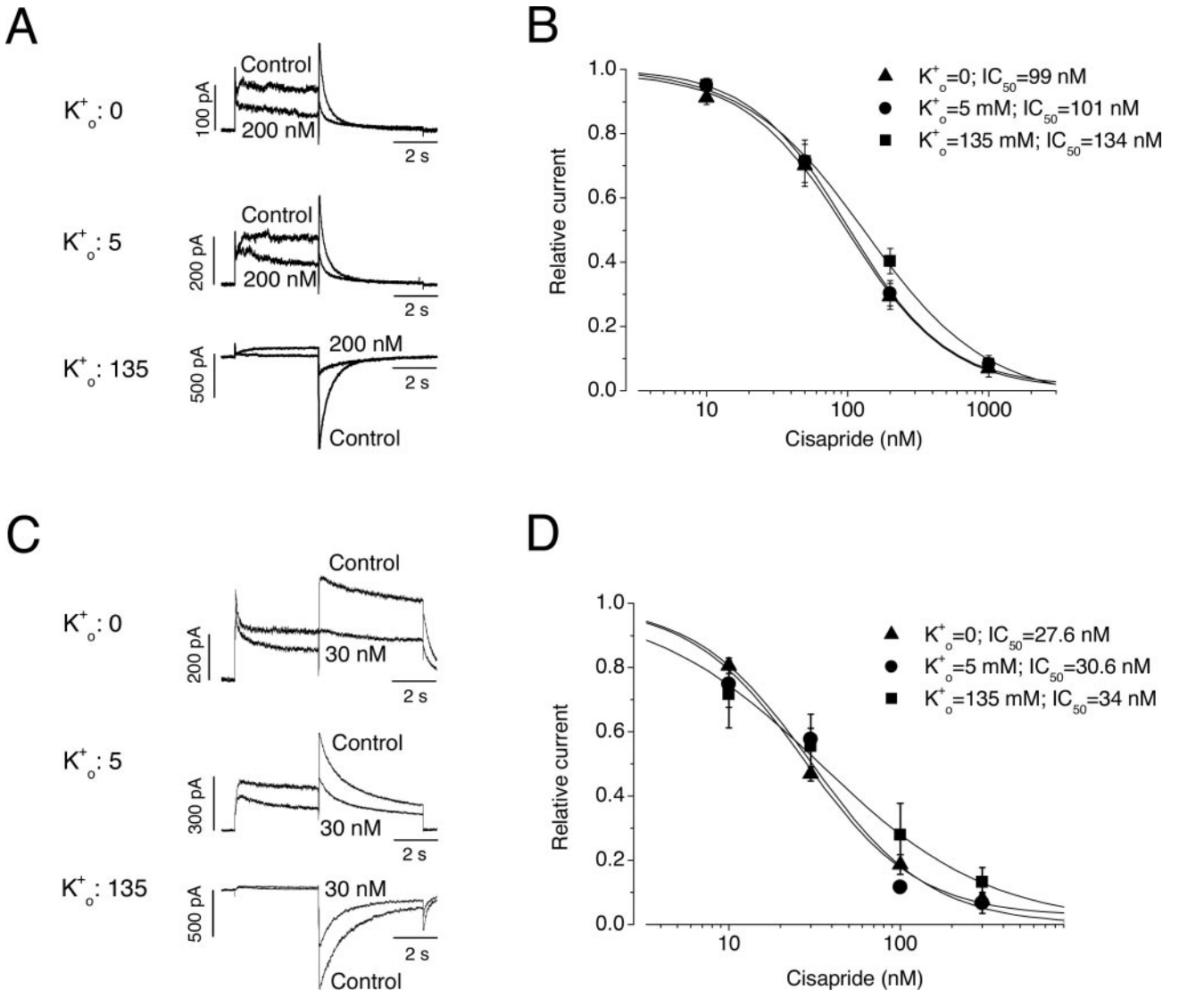

Fig. 8. Cisapride block of the F656V and F656M is not affected by $[K^+]_o$. A, the F656V K^+ currents in the absence and presence of 200 nM cisapride. From a holding potential of −80 mV, the channels were repetitively activated by a depolarization to +50 mV for 4 s followed by a repolarization to −50 mV to record tail currents. The interpulse interval was 15 s. The pipette solution contained 135 mM K^+ and the bath solution contained 0, 5, or 135 mM K^+. B, concentration-dependent block of F656V currents by cisapride at $[K^+]_o$ of 0 (▲), 5 (●), or 135 mM (■). Tail current amplitudes in the presence of cisapride were normalized to the control and plotted versus cisapride concentration. The data were fitted to the Hill equation. C, the F656M K^+ currents in the absence and presence of 30 nM cisapride. D, concentration-dependent block of the F656M currents by cisapride at $[K^+]_o$ of 0 (▲), 5 (●), or 135 mM (■).

K^+, inactivation gating no longer affects the cisapride-mediated block of HERG. With Cs^+ ions in the pipette solution, the IC_{50} values of cisapride were similar between the WT and inactivation-deficient S620T channels. Although elevation of extracellular Cs^+ concentration significantly slowed the Cs^+ current inactivation of WT HERG channels, it did not alter the cisapride block of HERG Cs^+ current. Furthermore, we observed that altering inactivation affects the IC_{50} of cisapride block of HERG less than does intracellular Cs^+ replacement and that Cs^+ replacement further reduced the IC_{50} of cisapride in the inactivation-deficient mutant channels. For example, whereas S620T inactivation-deficient mutation reduced the cisapride affinity by 6.6-fold in a bath solution containing 135 mM Na^+, under the same bath solution replacement of the intracellular $[K^+]_o$ by Cs^+ reduced the cisapride affinity of WT channels by 23-fold. Replacement of intracellular $[K^+]_o$ by Cs^+ also reduced the cisapride affinity of S620T inactivation-deficient channels by 4-fold (IC_{50} from 49.5 to 194.9 nM; Figs. 2 and 5) in a bath solution containing 0 K^+ and Cs^+ (135 mM Na^+). These results argue against inactivation as being the sole primary determinant of drug block.

The mechanism by which Cs^+ replacement affects cisapride block is not known but may be related to the positioning of the drug binding site. C-type inactivation reflects a stabilized P-type inactivation and S5–S6 arrangements might be involved in this process to affect the selectivity filter and adjacent structures. On the other hand, the permeant ions may modify the selectivity filter and adjacent structure (Zhou and MacKinnon, 2004). The occupancy of the selectivity filter by particular permeant ions might stabilize a conformation of the S5–S6 arrangement. We propose that the S5–S6 is stabilized by K^+ ions to a molecular state/position in which inactivation gating can further induce a conformational change that increases cisapride affinity to the channel. In contrast to K^+, Cs^+ stabilizes the S5–S6 in a different molecular state/position such that inactivation gating cannot increase cisapride affinity to the channel. Thus, in addition to direct interactions or via changes in channel inactivation, K^+ ions are also critical for maintaining a proper conformation of the channel required for drug-channel interactions.

In summary, we have found that both intracellular K^+ and Phe-656 are required for inactivation-related high-affinity cisapride binding to HERG. We propose that intracellular K^+ ions stabilize the HERG channel in a state in which inactivation can alter the receptor site of Phe-656 to a position that favors high-affinity cisapride binding. Our findings suggest a possible explanation for how inactivation gating facilitates drug affinity to HERG channels. It has been shown that block of Na^+ or Ca^{2+} channels by many drugs is facilitated by channel inactivation. Whether intracellular K^+ plays a role in the state dependent block of Na^+ or Ca^{2+} channels by drugs (Hille, 1977; Hondeghem and Katzung, 1984) requires further investigation.

Acknowledgments

We thank Dr. Craig January for the stable HERG cell line (Zhou et al., 1998) and Dr. Gail Robertson for the HERG cDNA (Trudeau et al., 1995).

References

Chen J, Seebohm G, and Sanguinetti MC (2002) Position of aromatic residues in the S6 domain, not inactivation, dictates cisapride sensitivity of HERG and Eag potassium channels. *Proc Natl Acad Sci USA* **99:**12461–12466.
Doyle DA, Cabral JM, Pfuetzner RA, Kuo AL, Gulbis JM, Cohen SL, Chait BT, and MacKinnon R (1998) The structure of the potassium channel: molecular basis of K^+ conduction and selectivity. *Science (Wash DC)* **280:**69–77.
Fernandez D, Ghanta A, Kauffman GW, and Sanguinetti MC (2004) Physicochemical features of the HERG channel drug binding site. *J Biol Chem* **279:**10120–10127.
Ficker E, Jarolimek W, Kiehn J, Baumann A, and Brown AM (1998) Molecular determinants of dofetilide block of HERG K^+ channels. *Circ Res* **82:**386–395.
Hille B (1977) Local anesthetics: hydrophilic and hydrophobic pathways for the drug-receptor reaction. *J of Gen Physiol* **69:**497–515.
Ho SN, Hunt HD, Horton RM, Pullen JK, and Pease LR (1989) Site-directed mutagenesis by overlap extension using the polymerase chain reaction. *Gene* **77:**51–59.
Hondeghem LM and Katzung BG (1984) Antiarrhythmic agents: the modulated receptor mechanism of action of sodium and calcium channel-blocking drugs. *Annu Rev Pharmacol Toxicol* **24:**387–423.
Keating MT and Sanguinetti MC (2001) Molecular and cellular mechanisms of cardiac arrhythmias. *Cell* **104:**569–580.
Kiehn J, Lacerda AE, Wible B, and Brown AM (1996) Molecular physiology and pharmacology of *HERG*–single-channel currents and block by dofetilide. *Circulation* **94:**2572–2579.
Lees-Miller JP, Duan Y, Teng GQ, and Duff HJ (2000) Molecular determinant of high-affinity dofetilide binding to HERG1 expressed in *Xenopus* oocytes: involvement of S6 sites. *Mol Pharmacol* **57:**367–374.
Mitcheson JS, Chen J, Lin M, Culberson C, and Sanguinetti MC (2000a) A structural basis for drug-induced long QT syndrome. *Proc Natl Acad Sci USA* **97:**12329–12333.
Mitcheson JS, Chen J, and Sanguinetti MC (2000b) Trapping of a methanesulfonanilide by closure of the HERG potassium channel activation gate. *J Gen Physiol* **115:**229–240.
Mohammad S, Zhou Z, Gong Q, and January CT (1997) Blockage of the HERG human cardiac K^+ channel by the gastrointestinal prokinetic agent cisapride. *Am J Physiol* **273:**H2534–H2538.
Roden DM, Lazzara R, Rosen M, Schwartz PJ, Towbin J, and Vincent GM (1996) Multiple mechanisms in the long-QT syndrome. Current knowledge, gaps and future directions. The SADS Foundation Task Force on LQTS. *Circulation* **94:**1996–2012.
Sanguinetti MC, Jiang C, Curran ME, and Keating MT (1995) A mechanistic link between an inherited and an acquired cardiac arrhythmia: *HERG* encodes the I_{Kr} potassium channel. *Cell* **81:**299–307.
Sanguinetti MC and Jurkiewicz NK (1990) Two components of delayed rectifier K^+ current. *J Gen Physiol* **96:**195–215.
Smith PL, Baukrowitz T, and Yellen G (1996) The inward rectification mechanism of the HERG cardiac potassium channel. *Nature (Lond)* **379:**833–836.
Snyders DJ and Chaudhary A (1996) High affinity open channel block by dofetilide of *HERG* expressed in a human cell line. *Mol Pharmacol* **49:**949–955.
Spector PS, Curran ME, Zou AR, and Sanguinetti MC (1996) Fast inactivation causes rectification of the I_{Kr} channel. *J Gen Physiol* **107:**611–619.
Suessbrich H, Schonherr R, Heinemann SH, Lang F, and Busch AE (1997) Specific block of cloned Herg channels by clofilium and its tertiary analog LY97241. *FEBS Lett* **414:**435–438.
Trudeau MC, Warmke JW, Ganetzky B, and Robertson GA (1995) HERG, a human inward rectifier in the voltage-gated potassium channel family. *Science (Wash DC)* **269:**92–95.
Trudeau MC, Warmke JW, Ganetzky B, and Robertson GA (1996) HERG sequence correction. *Science (Wash DC)* **272:**108719.
Wang S, Morales MJ, Liu S, Strauss HC, and Rasmusson RL (1997) Modulation of HERG affinity for E-4031 by $[K^+]_o$ and C-type inactivation. *FEBS Lett* **417:**43–47.
Yang T and Roden DM (1996) Extracellular potassium modulation of drug block of I_{Kr}. Implications for torsade de pointes and reverse use-dependence. *Circulation* **93:**407–411.
Zhang S, Kehl SJ, and Fedida D (2003a) Modulation of human Ether-a-go-go-related K^+ (HERG) channel inactivation by Cs^+ and K^+. *J Physiol (Lond)* **548:**691–702.
Zhang S, Kurata HT, Kehl SJ, and Fedida D (2003b) Rapid induction of P/C-type inactivation is the mechanism for acid-induced K^+ current inhibition. *J Gen Physiol* **121:**215–225.
Zhang S, Rajamani S, Chen Y, Gong Q, Rong Y, Zhou Z, Ruoho A, and January CT (2001) Cocaine blocks HERG, but not KvLQT1+MinK, potassium channels. *Mol Pharmacol* **59:**1069–1076.
Zhang S, Zhou Z, Gong Q, Makielski JC, and January CT (1999) Mechanism of block and identification of the verapamil binding domain to HERG potassium channels. *Circ Res* **84:**989–998.
Zhou Y and MacKinnon R (2004) Ion binding affinity in the cavity of the KcsA potassium channel. *Biochemistry* **43:**4978–4982.
Zhou Z, Gong Q, Ye B, Fan Z, Makielski JC, Robertson GA, and January CT (1998) Properties of HERG channels stably expressed in HEK 293 cells studied at physiological temperature. *Biophys J* **74:**230–241.

Address correspondence to: Dr. Shetuan Zhang, Institute of Cardiovascular Sciences, St. Boniface General Hospital Research Centre and Department of Physiology, Faculty of Medicine, University of Manitoba, 351 Tache Avenue, Winnipeg, Manitoba, Canada R2H 2A6. E-mail: szhang@sbrc.ca